

4 Tesla Gradient Recalled Echo Characteristics of Photic Stimulation-Induced Signal Changes in the Human Primary Visual Cortex

Ravi S. Menon, Seiji Ogawa, David W. Tank, Kâmil Uğurbil

Ravi S. Menon, Seiji Ogawa, David W. Tank, Kâmil Uğurbil

Multi-echo measurements of photic stimulation-induced signal changes in human visual cortex were made at 4 Tesla in order to quantify the nature of the signal change and its vascular origin, and to determine the optimum echo time for detection of the changes. Utilizing high resolution images, two distinct regions (ascribed to be microvasculature and visible venous vessels) were identified as giving rise to the signal increase. The fractional signal changes in gray matter areas depended linearly on echo time (TE) in the range of 10 to 60 ms and extrapolated to virtually zero for $TE = 0$, indicating that in-flow effects secondary to stimulation-induced blood flow increases were negligible in our functional imaging studies; instead, signal change due to photic stimulation originated from the increase in the apparent transverse relaxation rate, $1/T_2^*$. This decrease in $(1/T_2^*)$, brought about by the alterations in hemodynamic parameters, was $1.3 \pm 0.4 \text{ s}^{-1}$ for gray matter and $3.0 \pm 0.7 \text{ s}^{-1}$ (averaged over 10 individuals) for venous vessels visible in the images. The optimum choice of echo time was found to be $TE \approx T_2^*$.

Key words: functional MR; visual cortex; human brain function; human brain mapping.

INTRODUCTION

The signal intensity of T_2^* -weighted gradient recalled echo images display nominal 5–25% increases in the primary visual cortex during photic stimulation (1, 2). It has been postulated on the basis of positron emission tomography (PET) observations (3, 4) that this is due to an increase in regional cerebral blood flow (rCBF) with little or no increase in regional oxygen consumption; this results in a decrease in the amount of the intravascular endogenous paramagnetic contrast agent, deoxyhemoglobin, relative to the amount present in the vasculature in the baseline state. An elevation in venous oxygenation caused by a large increase in rCBF can result in decreased tissue magnetic susceptibility, overcoming the potential tissue susceptibility enhancement due to possible increases in cerebral blood volume (CBV) in the region. Consequently, stimulation causes signal intensity in-

creases in T_2^* -weighted MR images. The phenomenon by which deoxyhemoglobin alters image intensity in gradient recalled echo images has been termed blood oxygen level dependent (BOLD) contrast (5). In order to understand the nature of the NMR signal response upon stimulation in the human visual cortex, we have examined the signal response as a function of echo time with a FLASH sequence employing multi-echo data acquisition. Acquiring all echoes simultaneously eliminates errors due to variations of the visual cortex response from one stimulation period to the next as well as misregistration caused by motion between sequential experiments done at single echo times.

MATERIALS AND METHODS

All magnetic resonance imaging experiments were performed on a Siemens (Erlangen, Germany)/SIS Co. (Sunnyvale, CA) 4 T whole body system equipped with actively shielded gradients using either a snugly fitted quadrature driven surface coil or a quadrature head coil. To locate the visual cortex, anatomical T_1 -weighted images were acquired using a refocused FLASH gradient recalled echo sequence ($TE = 8 \text{ ms}$, $TR = 11 \text{ ms}$, and 0.33 cm slice thickness) with 256 phase-encoding steps segmented (to preserve contrast) in four blocks of 64 interleaved steps. An oblique plane lying in the calcarine fissure was defined from these sagittal images. Imaging during photic stimulation was performed either in a sagittal plane that clearly identified the calcarine fissure or in an oblique plane parallel to and containing the calcarine fissure. For generation of the functional "activation" maps, consecutive multiple-gradient-echo images (typically 20 control, 20 photic stimulation, and 20 recovery images at 4.3 s per image plus a 1.2-s inter-image delay) were acquired in either of the above-described imaging planes using a refocused, RF spoiled, multi-echo FLASH pulse sequence. The echoes spanned the range of 10 to 60 ms and were equally spaced. The field of view was either 16×16 (oblique) or $20 \times 20 \text{ cm}$ (sagittal) using 128 complex pairs in the read direction and 64 gradient increments in the phase encode dimension. The slice thickness was 0.33 cm. The acquired data were zero-filled to 256×256 points before Fourier transformation. On some subjects, functional imaging was also performed with the same protocol using several discrete echo times rather than a multiecho sequence. In addition, multislice 256×256 point FLASH images were acquired over the same fields of view and in planes parallel to and including the multi-echo functional imaging plane, using a TE of 15 to

MRM 30:380–386 (1993)

From the Center for Magnetic Resonance Research (CMRR), University of Minnesota Medical School, Minneapolis Minnesota and the Biological Computation Research Department, AT&T Bell Laboratories, Murray Hill, New Jersey (S.O., D.W.T.)

Address correspondence to: Ravi S. Menon, Ph.D., Center for Magnetic Resonance Research, University of Minnesota Medical School, 385, East River Road, Minneapolis, MN 55455.

Received April 14, 1993; revised June 10, 1993; accepted June 24, 1993.

This work was supported by NIH grants RR08079, HL33600 and a fellowship to R.M. from the Alberta Heritage Foundation for Medical Research.

0740-3194/93 \$3.00

Copyright © 1993 by Williams & Wilkins

All rights of reproduction in any form reserved.

17 ms and a TR of 20 to 22 ms. These images, which we will refer to as "high resolution T_2^* -weighted" images, were acquired with a tip angle of 45° and were used to discern large venous vessels from large arterial vessels and the sagittal sinus. In these images, venous vessels (except for the fast flowing very large sinuses such as the sagittal sinus) appear as dark lines or spots due to signal loss caused by deoxyhemoglobin-induced susceptibility effects and consequent dephasing (5-7), the phenomenon that gives rise to the BOLD effect. The arterial vessels and the sinuses appear bright due to the fast flowing spins. The purpose of these images was to identify venous vessels which could give rise to changes in the BOLD effect due to photic stimulation, and not to perform a comprehensive angiography study. Venous vessels that are parallel to the static magnetic field would not show up in these high resolution T_2^* -weighted images unless their flow is very fast as in the sagittal sinus, but neither would they give rise to a BOLD effect by virtue of their orientation. Flow compensation was not used in any of the sequences.

For functional imaging, an alternating phase-encoding scheme was employed, with the zero phase-encode gradient being acquired first, followed by increasingly higher order k -space values ($\pm 1, \pm 2, \dots$). For the T_1 -weighted FLASH images, a similar scheme was used, with each interleaved segment of k -space, starting with a low k -space value. High resolution imaging was implemented with a conventional linear phase encoding table. Images acquired with an alternating phase-encoding strategy are expected to be less sensitive to in-flow than conventionally acquired images, as explained in the discussion below.

Photic stimulation was accomplished with LED goggles manufactured by Grass Instruments (Quincy, MA) at a frequency of 8 Hz. Shimming in the region of the primary visual cortex was accomplished by slice-selective shimming. Line widths of 15 Hz were routinely achievable. Magnetization decay curves from a region of interest (ROI) were fitted with the robust non-negative least-squares (NNLS) technique of Lawson and Hanson (8) as modified in (9). Images made on small bottles of tap water showed excellent exponential decay characteristics through the eight echoes, indicating that eddy-currents were not significantly affecting the behavior of the magnetization.

RESULTS AND DISCUSSION

For each echo time, a baseline image was generated by performing an average on a pixel-by-pixel basis of all pre- and poststimulation images. Additionally, for each echo time, a standard deviation image was constructed from the 40 nonstimulus images based on the variance and mean for each pixel. Similar average and standard deviation images were generated for the stimulation period. An activation map was obtained by subtracting the baseline image from the stimulation image, and all pixels in the difference map, which did not exceed three standard errors, were set to zero. Additionally, a given ROI could

be followed through each of the consecutive images, generating a time course for the ROI.

(i) Spatial Assignment of Signal Changes

The areas activated according to the above procedure could be classified into two distinct types of regions on the basis of the high-resolution, T_2^* -weighted images and the T_1 -weighted images. This distinction is illustrated with the images presented in Fig. 1. Figure 1a displays a high resolution T_2^* -weighted image; Figs. 1b and 1c illustrate the activation map due to photic stimulation for the 32.5-ms echo superimposed on the T_2^* - and T_1 -weighted images, respectively. The first type of region where the activation is noted accounts for most of the large percentage changes upon photic stimulation but is highly localized. Examination of the corresponding location of these "hot-spots" in the high resolution T_2^* images (e.g., Fig. 1a) shows the presence of very dark areas that have the appearance of either roughly circular spots or lines; some of these dark areas (spots and lines) are identified with arrows in Fig. 1a. The second type of activated region is more diffuse in nature, accounting for most of the spatial extent of the activation. The corresponding locations in the high-resolution T_2^* -weighted FLASH images show little if any remarkable features. A characteristic of these T_2^* -weighted images is that the gray matter appears somewhat darker than the white matter, presumably because of the influence of the deoxyhemoglobin laden capillaries which are denser in the gray matter than in the white matter (5-7). Figure 1 indicates that most of the "hot spots" are located over the dark areas (spots or lines) in the T_2^* -weighted image and that these regions correspond to the fissures in the T_1 -weighted images. In contrast, the "activated" diffuse areas appear to lie more on the gray matter lining the fissure rather than directly on the fissure.

Figures 2a-c illustrate similar data obtained in an oblique plane. The yellow arrows identify some areas with obvious dark spots in the high-resolution T_2^* -weighted FLASH images and the red arrows indicate some bright spots and lines which we associate with arterial vessels. As in Fig. 1, the "hot spots" of activation appear to lie on the very dark regions in the T_2^* -weighted images, while the rest of the activation appears to be solely in gray matter. Careful spatial analysis indicates that little if any activation can be ascribed to the arterial spins.

Typical exponential decay curves from the sum of each of these two types of regions in Fig. 2 are shown in Fig. 3a. One of the curves is obtained from a summation of the signal from all the activated areas associated with dark spots and the other curve is from the remaining spatially diffuse activation in the primary visual cortex of the volunteer. These decay curves display single exponential behavior within the range of echo times used in these experiments (albeit with different T_2^* values), indicating that there is no interference between the magnetic fields due to eddy currents and the tissue local magnetic field gradients. NNLS fitting of the magnetization decay curves from experiments on 10 individuals yielded a resting state gray matter T_2^* value of 30 ± 4 ms and a

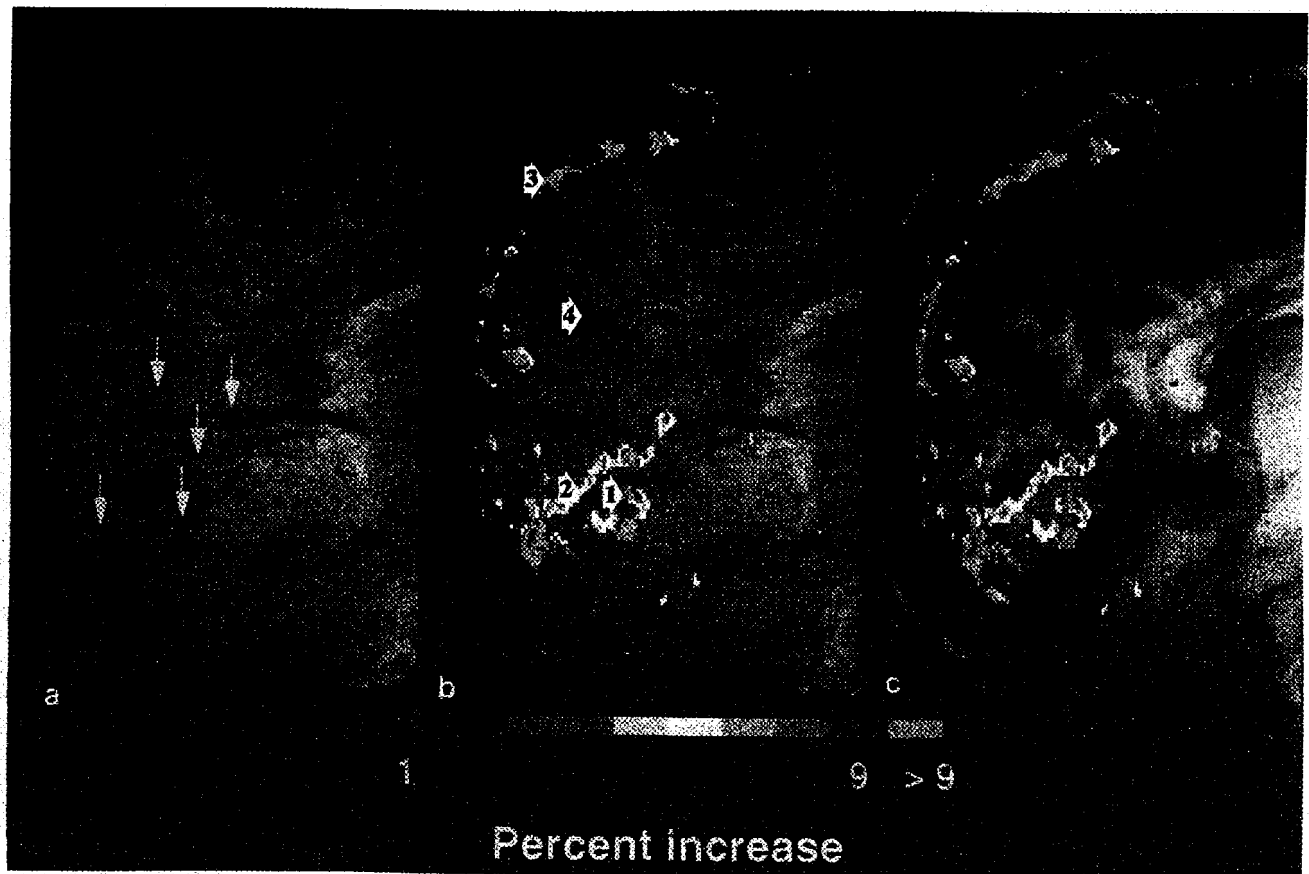


FIG. 1. Example of a sagittal study at a discrete echo time. (a) High resolution T_2^* weighted FLASH image ($TE = 15$ ms/ $TR = 20$ ms) acquired with 256 by 256 points over a 20×20 cm field of view and with a 0.33-cm slice. The yellow arrows point to some of the large veins. Also apparent is some gray-white matter contrast. (b) An overlay on top of (a) using the zero-filled 128×64 point activation map acquired with an echo-time of 32.5 ms using the same field of view and slice parameters as in (a). (c) An overlay of the same activation map as in (b) on top of the 256×256 T_1 -weighted FLASH image showing gray-white matter differentiation using the same field of view and slice parameters as in (a).

resting state localized dark areas T_2^* of 20 ± 3 ms. Upon stimulation, a change in the apparent relaxation rate ($\Delta(1/T_2^*)$) of 1.3 ± 0.4 s⁻¹ was found for the gray matter areas and a $\Delta(1/T_2^*)$ of 3.0 ± 0.7 s⁻¹ was found for the dark spots and lines.

We conclude that the very dark lines and spots detected in the high resolution T_2^* -weighted images arise from some of the venous vessels in the human brain and we refer to these as the "macrovasculature." This conclusion is based on the following observations: a) These dark spots and lines have a shorter T_2^* leading to their dark appearance, as expected from venous vessels and as demonstrated in earlier rat brain studies (5, 6), b) they display higher variance (in the standard error images) consistent with more pulsatility than the surrounding tissue, c) when followed in contiguous multislice high resolution T_2^* -weighted images, these very dark spots and lines form blood vessel-like structures where some of the well-known large venous vessels of the human brain can be easily recognized. We note that these dark spots and lines are not always apparent in the T_1 -weighted images due to the short TE of the magnetization prepared TurboFLASH sequence and since the veins often lie along the fissures,

which also appear dark with our chosen inversion time. Thus, some of the very high intensity changes in the functional maps are associated with relatively large venous vessels. The remainder of the activation, we associate with the gray matter tissue in which the blood vessels (capillaries, venuoles, and submillimeter diameter veins which we collectively term the "microvasculature") are much smaller than the spatial resolution of the high resolution T_2^* -weighted images. Further support for our assignment of activated areas comes from recent rat brain studies (10) where it was demonstrated that larger fractional changes occur in larger vessels versus the microvasculature for a given perturbation in vessel oxygenation. We have taken care in all cases to ensure that the stimulated slice corresponds exactly to one of the high-resolution T_2^* - and T_1 -weighted slices. Because we also obtained contiguous multislice high-resolution FLASH data, we were able to easily follow the path taken by the veins to rule out partial volume effects in the slice chosen for the stimulation effect.

It should be noted that the subject in Fig. 1 was investigated with several discrete echo times, while the subject in Fig. 2 was investigated with the multi-echo sequence.

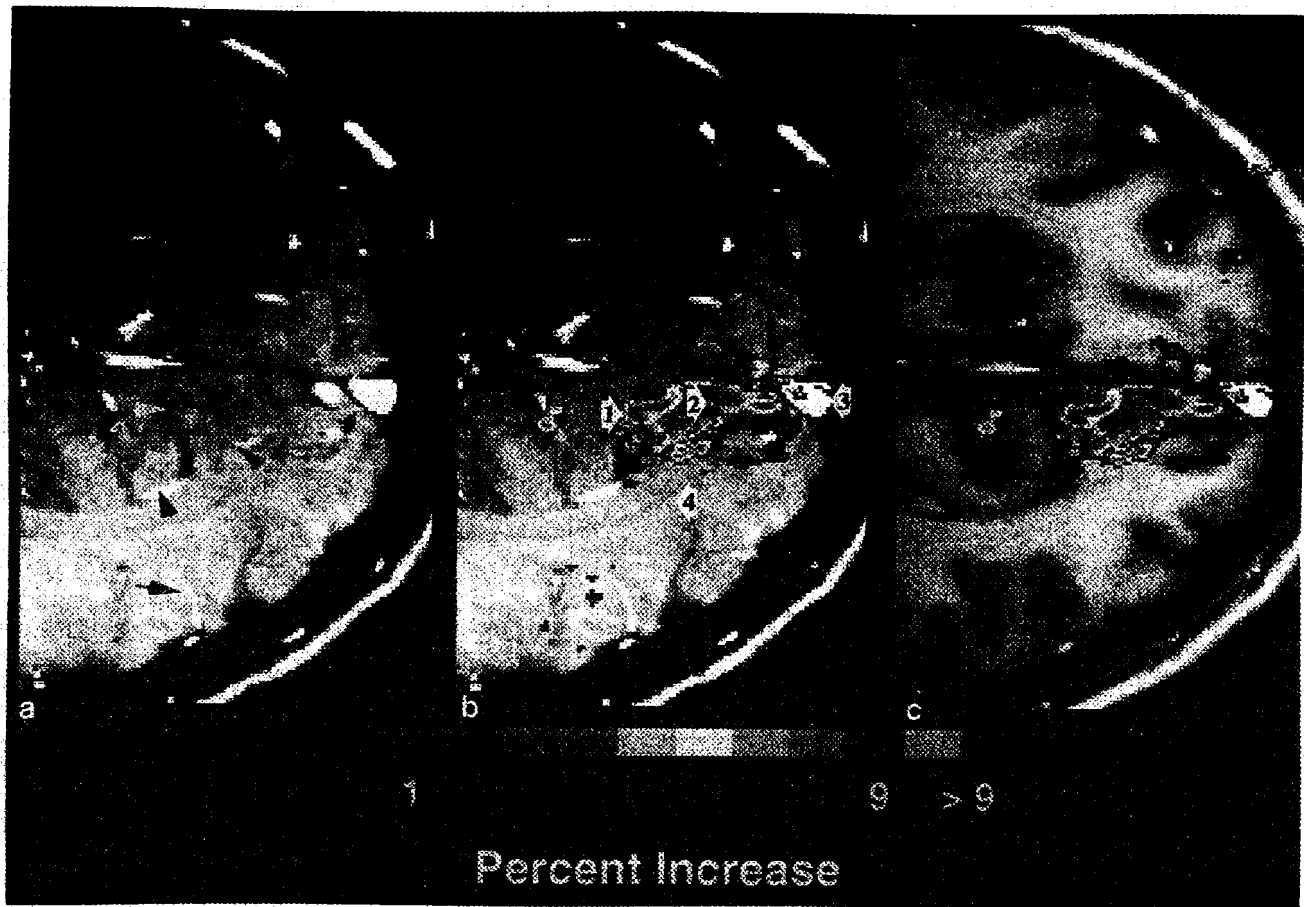


FIG. 2. Example of a multi-echo oblique study in the calcarine fissure (third-echo activation map shown). (a) High resolution T_2^* -weighted FLASH image ($TE = 17$ ms/ $TR = 22$ ms) acquired with 256×256 points over a 16×16 cm field of view and with a 0.33-cm slice. The yellow arrows point to some of the large veins. The red arrows identify some of the bright arterial vessels. Also apparent is some gray-white matter contrast. (b) An overlay on top of (a) using the zero-filled 128×64 point activation map derived from the third echo (32.3 ms) using the same field of view and slice parameters as in (a). (c) An overlay of the same activation map as in (b) on top of the 256×256 T_1 -weighted FLASH image showing gray-white matter differentiation using the same field of view and slice parameters as in (a).

The activation maps shown are for almost identical echo-times. No quantitative differences can be found between the two methods as far as the behavior of the time courses are concerned (see section iii below). However, there was considerably more spread in the magnetization decay values in the discrete approach, as expected due to subject motion and the variation in subject response from one stimulation episode to the next.

(ii) Expressions for Echo-Time-Dependent Signal Change and Contrast-to-Noise

In such images where the intrinsic pixel resolution is coarse compared to the spatial variation of the magnetic susceptibility of the blood in the microvasculature, the pixel intensity (S) in a gradient recalled echo MR image made at an echo time of TE can be expressed as

$$S = S_0 \exp(-TE/T_2^*) \quad [1]$$

since our data (such as Fig. 3a) show no evidence of multiexponential behavior. Utilizing Eq. [1] we can derive an expression for the fractional change in signal

intensity upon stimulation ($\Delta S/S$).

$$1 + (\Delta S/S) = \exp(-TE(\Delta(1/T_2^*)))$$

or since $(TE(\Delta(1/T_2^*)) \ll 1)$

$$\Delta S/S = -TE(\Delta(1/T_2^*)). \quad [2]$$

This essentially linear behavior is clearly evident for the tissue region in Fig. 3b, which shows the experimentally measured values of $\Delta S/S$ as a function of the eight echoes used in the experiment for the same regions of gray matter shown in Fig. 2. Again, one should note that the difference between baseline and stimulation curves at the zero time intercept is not significantly different, indicating that the effect giving rise to the increase in pixel intensity in the image is solely a T_2^* effect and not brought about by an increased flow in the capillary and venous side vasculature. For the venous vessels we observe a stronger dependence of $\Delta S/S$ upon TE as expected, but a deviation from linearity at longer echo times, possibly due to S for the vessels approaching the noise threshold at longer echo times. While the quantity $\Delta S/S$ is a continuously increasing function of echo time,

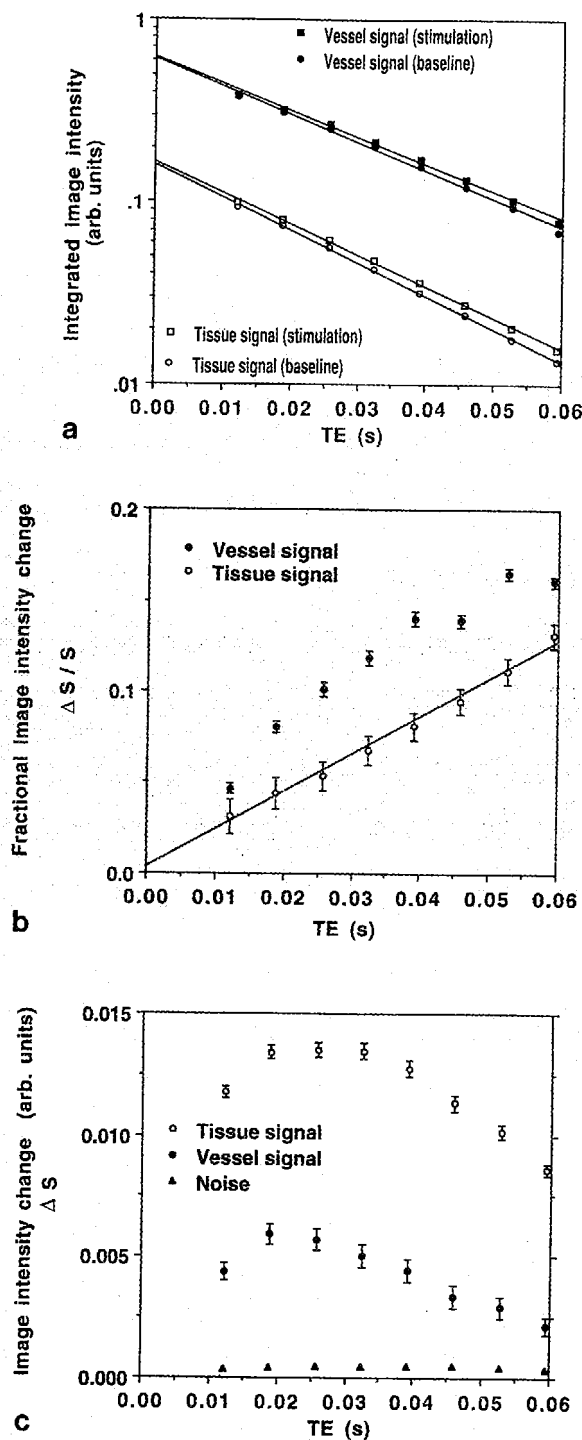


FIG. 3. (a) Decay of transverse magnetization in a multiple gradient recalled echo imaging sequence during baseline and stimulation conditions. The volume of interest from which the data are obtained is described in the text and comes from Fig. 2. The lines indicate the NLS fit to each decay curve. T_2^* of the tissue is 28 ± 2 ms and T_2^* of the vessel regions is 20 ± 2 ms. Upon stimulation, only the slope of the lines change significantly indicating a change in the relaxation rate. (b) A plot of the difference in image intensity (ΔS) between stimulation and control states, normalized to the control state (S), as a function of the echo time. Note that the tissue contribution is linear with echo time, but that the venous vessel contribution has a stronger dependence on TE and appears to level out or even drop

the quantity ΔS (the relevant parameter in a difference image) has a maximum due to the fact that the tissue signal, S , is decreasing with echo time. Replacing S in Eq. [2] with Eq. [1] and differentiating with respect to TE shows that the maximum achievable value of ΔS occurs at TE equal to T_2^* . Figure 3c demonstrates this for data obtained experimentally. Of course TE equal to T_2^* is the optimum for generating functional maps only if the absolute image fluctuations are independent of echo time. To verify this we also plot the baseline standard error in the gray matter areas as a function of echo time in the figure. This standard error is virtually invariant with echo time. Thus, barring echo-time dependent problems of instrumental origin, $\Delta S/\text{noise}$ (contrast-to-noise) is expected to have a maximum at $TE = T_2^*$ and this condition is achieved in our studies.

(iii) Analysis of the Time Course Data

In Fig. 4 we illustrate the time course of signal changes in selected regions during photic stimulation from the subjects shown in Figs. 1 and 2. These regions are chosen to be roughly anatomically equivalent between the two subjects. Region 1 corresponds to a visible but small venous vessel in both high resolution maps (Figs. 1a, 2a). This region gives rise to changes of 27% and 17%, respectively, in each of the two subjects. Region 2 for both subjects, lies in an area with no visible vasculature and accounts for changes of 8% and 7%, respectively, at essentially the same echo-times. Region 3 lies in the sagittal sinus of both subjects and exhibits a different behavior in the two different studies. For Region 3, there appears to be clear activation in the sagittal study of Fig. 1, while in the oblique-axial study of Fig. 2 there is no apparent change. The difference lies in the fact that the sagittal sinus is parallel to the static magnetic field at its anatomic location in Fig. 2 and therefore does not exhibit a BOLD effect. In the sagittal study, the region of the sinus which is parallel to the field also exhibits little change in signal intensity upon stimulation, but a pronounced BOLD effect is seen (as a line that appears to be outside the brain but following its outer contours) once this sinus curves away from being parallel to the static magnetic field. We notice that Regions 1 and 2 in both studies exhibit an as yet unexplained undershoot below the pre-stimulus baseline for a period of ~ 15 s after the stimulation as we first reported in (2).

Region 4 lies in white matter for both images and does not exhibit any activation as expected. Interestingly, the fluctuations in the white matter are consistently lower than in gray matter, which in turn has less "noise" than the visible venous vessels. The traces exhibiting the most

at longer TE values. (c) A plot of the difference in image intensity (ΔS) between stimulation and control states. This graph was calculated from the data in (a), as a function of the echo time. Note that the peak for the tissue signal is found at $TE \sim 28$ ms while the peak for the venous vessels is found at $TE \sim 20$ ms, consistent with their T_2^* values as discussed in the text. Also shown is the baseline standard error for a gray matter region, demonstrating constant absolute image intensity fluctuations as a function of echo time.

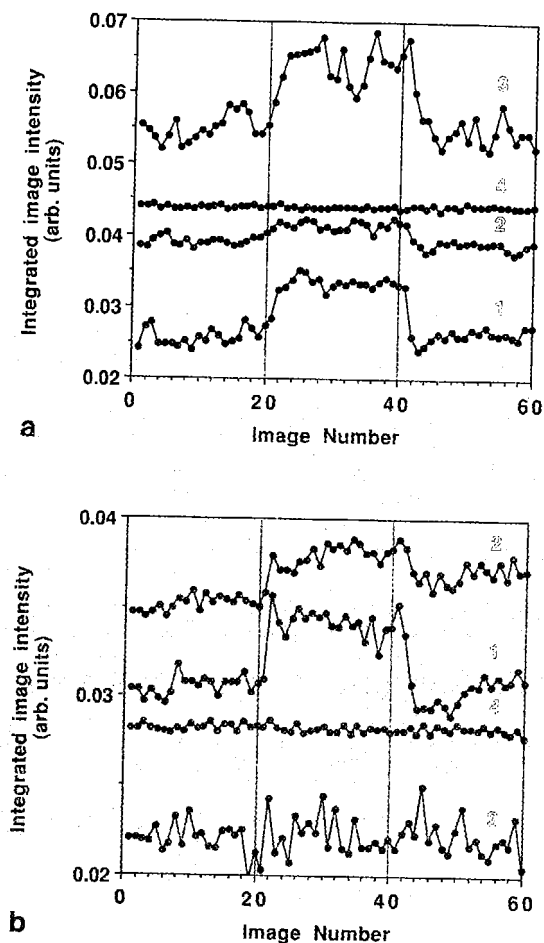


FIG. 4. Time course of the data from selected regions of Figs. 1 and 2. (a) Experimental time course obtained from the functional imaging experiment at the four anatomic regions marked in Fig. 1b. Region 1 corresponds to a large venous vessel, Region 2 to an area with no visible vessels, Region 3 to the sagittal sinus, and Region 4 lies in white matter. The intensities depend on the size of the ROI from which the data were integrated. (b) Experimental time course obtained from a functional imaging experiment at the four anatomic regions marked in Fig. 2b. The numbers above the traces correspond to the same regions described in (a).

fluctuation are those derived from the sinuses. This increase in noise going from poorly vascularized to vascular regions is thought to be related to the pulsatility of the blood supply caused by heart and respiration. Consequently, the standard error of the baseline images is higher for regions (but similar for all such regions) which are coded pink in the activation maps of Figs. 1 and 2. This may provide an additional method for differentiating signal changes associated with the microvasculature versus the macrovasculature and thus improve the specificity of the functional imaging technique.

The images in this and similar studies from our laboratory are acquired starting with the zero phase-encode gradient value in functional studies and this phase-encoding step contributes most of the signal intensity in the Fourier transformed image. Every image is preceded by a 1.2-s delay, which allows the static and flowing magnetization in the slice to recover considerably. This delay is

essential to reducing the flow sensitivity of our sequence. Since most of the water in the larger vessels is replenished by flow in this interimage delay time, we tend not to see strong flow effects in these vessels. In a conventional phase-encoding scheme, the flowing magnetization approaches a steady state governed by the TR of the FLASH sequence since the zero phase-encoding step is displaced in time by half the number of phase-encode values. This TR is of the order of tens of milliseconds and gives rise to significant saturation even in the larger vessels. Thus, increases in flow upon stimulation can give rise to considerable increases in image intensity in the macrovasculature, complicating the interpretation of the functional map.

CONCLUSIONS

Although the measurement of these signal changes is rather simple, i.e., gradient echo image acquisition in rapid succession, the nature of these signal change is complex. We are able to verify that, in our studies, the dominant reason for the signal increase upon stimulation is due to decreased T_2^* effects. Furthermore, we demonstrate that the signal changes can be grouped as arising from either relatively large venous vessels that can be visualized in the MR images (macrovasculature) or from areas in gray matter not associated with obvious large vessels; in the latter case, the origin of the signal change is presumably the venous microvasculature. These different areas also have significantly different changes in $1/T_2^*$ upon activation. In either case, the fractional signal change, $\Delta S/S$, increases with echo time, but the difference is maximized by using an echo time equal to the value of the T_2^* . Thus, the relative $\Delta S/\text{noise}$ of the venous vessel versus the diffuse gray matter contribution can be somewhat shifted toward the latter by going to longer echo times, while the short echo times emphasize the changes in the large vessels.

The T_2^* alterations are expected to have a dependence on magnetic field that is between linear and quadratic (7, 11). If we assume the conservative case of linear dependence and extrapolate downwards to 1.5 T, at the echo times used in this study, $\Delta S/S$ will be 1–2% in the gray matter areas and 5–6% in the relatively larger venous vessels. Therefore, it is likely that 5% or greater changes reported at 1.5 to 2 T (12–14) with relatively short echo times compared to T_2^* correspond to regions of large venous blood vessels or arise as a result of inflow effects associated with the large vessels, and are not activated gray matter areas; such regions, however, may be difficult to differentiate from the gray matter areas since large veins often run on the surface of the cortical gray matter.

It is therefore critical that the vasculature is mapped out in the region being examined by MR functional imaging. T_2^* signal changes corresponding to large veins in the interrogated slice may not reflect local tissue function, but may reflect instead neuronal activity in a region upstream of the vein. Additionally, when using linear phase-encoding schemes and FLASH, the stimulation induced changes in in-flow are most pronounced in the

macrovasculature and can confuse the interpretation of the activation map.

ACKNOWLEDGMENTS

The authors thank Dr. Hellmut Merkle for designing and building the RF surface coil that was used in some of these studies.

REFERENCES

1. K. K. Kwong, J. W. Belliveau, D. A. Chesler, I. E. Goldberg, R. M. Weisskoff, B. P. Poncelet, D. N. Kennedy, B. E. Hoppel, M. S. Cohen, R. Turner, H.-M. Cheng, T. J. Brady, B. R. Rosen, *Proc. Natl. Acad. Sci. (USA)* **89**, 5675 (1992).
2. S. Ogawa, D. W. Tank, R. S. Menon, J. M. Ellermann, S.-G. Kim, H. Merkle, K. Ugurbil, *Proc. Natl. Acad. Sci. (USA)* **89**, 5951 (1992).
3. P. T. Fox, M. E. Raichle, *Proc. Natl. Acad. Sci. (USA)* **83**, 1140 (1986).
4. P. T. Fox, M. E. Raichle, M. A. Mintun, C. Dence, *Science* **241**, 462 (1988).
5. S. Ogawa, T. M. Lee, A. R. Kay, D. W. Tank, *Proc. Natl. Acad. Sci. (USA)* **87**, 9868 (1990).
6. S. Ogawa, T. M. Lee, A. S. Nayak, P. Glynn, *Magn. Reson. Med.* **14**, 68 (1990).
7. R. Turner, P. Jezzard, H. Wen, K. K. Kwong, D. Le Bihan, T. Zeffiro, R. S. Balaban, *Magn. Reson. Med.* **29**, 277 (1993).
8. C. L. Lawson, R. J. Hanson, in "Solving Least Squares Problems," Prentice-Hall, Englewood Cliffs, NJ, 1974.
9. R. S. Menon, P. S. Allen, *Magn. Reson. Med.* **20**, 214 (1991).
10. S. Ogawa, T. M. Lee, B. Barrere, *Magn. Reson. Med.* **29**, 205 (1993).
11. S. Ogawa, R. S. Menon, D. W. Tank, S.-G. Kim, H. Merkle, J. M. Ellermann, K. Ugurbil, *Biophys. J.* **64**, 803 (1993).
12. J. Frahm, K.-D. Merboldt, W. Hanicke, *Magn. Reson. Med.* **29**, 139 (1992).
13. R. T. Constable, G. McCarthy, T. Allison, A. W. Anderson, J. C. Gore, *Magn. Reson. Imaging* **11**, 451 (1993).
14. L. R. Schad, U. Trost, M. V. Knopp, E. Muller, W. J. Lorenz, *Magn. Reson. Imaging* **11**, 461 (1993).